HYDROGEN COMPATIBILITY OF AUSTENITIC STAINLESS STEEL TUBING AND ORBITAL TUBE WELDS

Hughes, L.A.[1], Somerday, B.P.[1] Balch, D.K.[1] and San Marchi, C.[1]
[1] Sandia National Laboratories, 7011 East Ave., Livermore CA 94550 USA

ABSTRACT

Refueling infrastructure for use in gaseous hydrogen powered vehicles requires extensive manifolding for delivering the hydrogen from the stationary fuel storage at the refueling station to the vehicle as well as from the mobile storage on the vehicle to the fuel cell or combustion engine. Manifolds for gas handling often use welded construction (as opposed to compression fittings) to minimize gas leaks. Therefore, it is important to understand the effects of hydrogen on tubing and tubing welds. This paper provides an overview of work at Sandia National Laboratories on hydrogen compatibility of high-pressure tubing and orbital tube welds of several austenitic stainless steels.

1.0 INTRODUCTION

Hydrogen manifolds, for example in gaseous hydrogen fuel systems, predominantly use austenitic stainless steel tubing for processing and transporting hydrogen. In assembling a manifold, welding is one way in which potential leaks can be avoided (e.g., leaks associated with compression fittings). However, welds are known to be more sensitive than the base material to environmental effects due to the microstructure of the weld region [1, 2]. Since gaseous hydrogen is an environment that embrittles many structural alloys, there is a concern that welds in gaseous hydrogen manifolds may be more severely affected by hydrogen than the tubing base material.

Gaseous hydrogen effects on austenitic stainless steels have been extensively evaluated for many decades [3-9]. Nickel content, for example, affects resistance of austenitic stainless steels to hydrogen-assisted fracture, as demonstrated by the reduction of ductility from both internal and external hydrogen exposure during tensile tests [5, 7, 8]. The strength of austenitic stainless steels can be controlled by strain-hardening processes, which also affects resistance to hydrogen-assisted fracture [10]. Additional environmental factors, such as temperature exposure, influence hydrogen-assisted fracture as well. Studies show reduction of tensile ductility in the presence of hydrogen reaches a maximum around 220K for austenitic stainless steels [4, 5]. However, there are relatively few studies analyzing the role of microstructure on hydrogen-assisted fracture, and fewer studies analyzing the hydrogen effects on the weld microstructure [1, 2]. Microstructural effects due to processing may also be important to the performance of austenitic stainless steels when exposed to hydrogen. Precipitation of carbides at grain boundaries during thermal exposure (as experienced during welding, for example) is generally referred to as sensitization and has been shown to reduce tensile ductility of austenitic stainless steels exposed to hydrogen [6, 11-13].

This manuscript provides an overview of several active studies assessing hydrogen-assisted fracture of austenitic stainless steel tubing and orbital tube welds. The materials and microstructures explored in these studies reflect tubing and tubing welds intended for service with gaseous hydrogen. The studied materials are type 316L and several types of 304/304L austenitic stainless steels. All tubing was tested in tension in the as-received condition and after hydrogen precharging. Additionally, tubing with an orbital tube weld in the gauge length was tested. Selected tubing materials were also annealed or sensitized to evaluate the effects of microstructural changes on hydrogen-assisted fracture. The majority of testing was conducted at room temperature, with a few materials and conditions evaluated at temperature of 223K.

2.0 MATERIALS AND EXPERIMENTAL PROCEDURE

All of the materials described in this report are commercially available austenitic stainless steel tubing: one type 316L material, five type 304L materials and one type 304 material (the designation of L-

Table 1. Composition of austenitic stainless steels in this report, as specified by the manufacturer. The ID is the number used to designate the material in the text and *n/r* means this information is not reported on the material certification.

Alloy type	ID	Cr	Ni	Mn	Mo	Si	C	S	P
316L	–	16.7	12.4	1.7	2.1	0.39	0.018	0.006	0.027
304L	1	18.2	9.1	1.0	*n/r*	0.50	0.020	0.004	0.027
304L	2	18.6	11.7	1.7	0.08	0.43	0.021	0.0004	0.017
304L	3	18.7	11.6	1.6	*n/r*	0.50	0.015	0.026	0.032
304	4	18.3	10.2	0.74	0.29	0.33	0.04	0.002	0.033
304L	5	18.4	10.2	1.2	*n/r*	0.35	0.01	0.007	0.029
304L	6	18.4	8.2	1.1	*n/r*	0.46	0.024	0.003	0.028

grade in this report is based on carbon content <0.03 wt%, although some of the materials are dual certified to both type 304 and type 304L). The composition of the alloys is given in Table 1. The type 316L tubing was obtained in the nominally annealed condition with nominal outer diameter (OD) of 6.35 mm and nominal wall thickness of 1.24 mm. This material, however, is not fully annealed as the yield strength is almost 290 MPa. The six type 304/304L tubing materials all have a nominal OD of 3.18 mm with a nominal wall thickness of 0.71 mm; they are referred to as materials 1 through 6 (Table 1). The type 304 tubing is material 4. Three of the tubing materials were procured in the strain-hardened condition, while the other three were nominally annealed. The measured OD and measured inner diameter (ID) are used for all stress calculations.

Material 2 (strain-hardened type 304L, referred to as condition A) featured a relatively fine, equiaxed microstructure. It was additionally heat treated to produce five different microstructural variations with the same composition. They are: partially recovered (condition B: 866K / 60 min), nominally recovered (condition C: 1000 K / 30 min), partially recrystallized (condition D: 1033 K / 30 min), nominally recrystallized (condition E: 1116K / 60 min), and fully annealed (condition F: 1311 K / 60 min). In addition, all six type 304/304L tubing materials were subjected to a sensitization heat treatment at a temperature of 998K for 240 minutes. This heat treatment is not a typical sensitization heat treatment, but rather selected to represent a longer-term exposure to condition C.

Orbital tube weld specimens were formed by welding together two pieces of tubing, each 50 to 55mm long. The welding was performed with automated commercial tube welding equipment using standard vendor recommended practices (single-pass, gas tungsten arc welding). Two sets of welded type 316L tubing were prepared on different equipment with different operators, referred to as weld process A and weld process B. Welded type 304L tubing specimens were also prepared after heat treatment of material 2 from three conditions: condition A (strain-hardened), condition C (recovered), and condition F (annealed). The welding equipment and operator for the welded type 304L specimens were different from the type 316L processes. All welded tubing was tested in the as-welded condition without modification or machining of the welds.

Tensile testing was performed using approximately 100 mm long specimens (tubes or orbital tube welds) clamped over a length of approximately 25 mm on both ends using wedge grips. The gauge length between the grips was thus approximately 50 mm. To prevent the specimen from being crushed in the grips, round pin inserts were used (refer to ASTM E8); the length of the pin within the tubing specimens was approximately 25 mm, mirroring the length of the gripped section on each end of the specimen. Tests were conducted in laboratory air at room temperature (293 K) on a servo-hydraulic test frame. For selected materials and conditions, tensile testing was also conducted at subambient temperature of 223 K on an electromechanical test frame with a commercial temperature chamber using evaporated liquid nitrogen to maintain temperature. The temperature of the specimen was

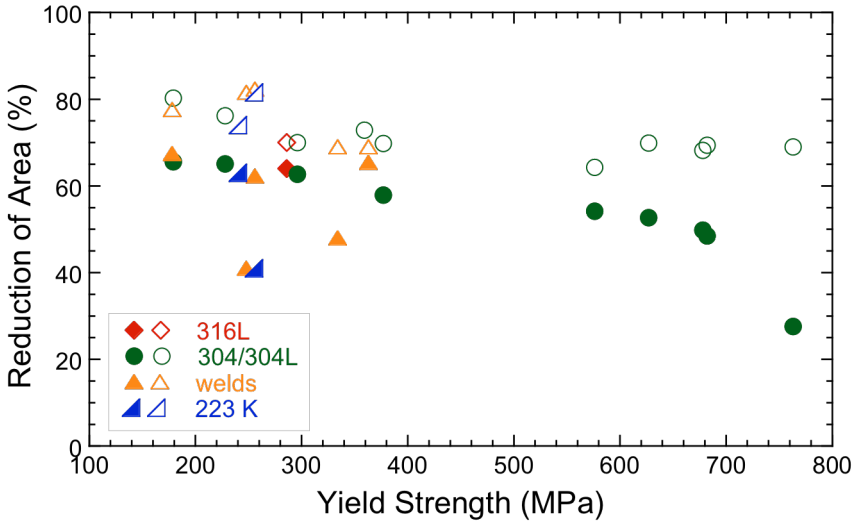

Figure 1. Reduction of area as a function of yield strength for all tested materials, with the exception of sensitized materials. Open symbols represent noncharged materials, while closed symbols represent hydrogen-precharged materials.

monitored throughout the low-temperature tests using thermocouples attached to the upper grip, lower grip, and the center of the tube.

An extensometer with a gauge length of 25.4 mm was centered in the gauge section and used to determine strain during testing. All testing was conducted at a constant displacement rate of 2.54 mm/min, which corresponds to a measured strain rate in the extensometer gauge of about 5 x 10^{-4} s^{-1}. The nickel content, carbon content, 0.2% offset yield strength (YS), and reduction of area (RA) are used to characterize the mechanical properties of the tested materials and conditions. RA values were determined with the aid of digital stereo-images at 30X using commercial software to correct for focal distance. For comparison of the tensile ductility with and without hydrogen the relative reduction of area (RRA) is sometimes used: RA with internal hydrogen relative to the RA of the same tubing material and condition without hydrogen.

A uniform saturation of hydrogen within the specimens was achieved by thermal precharging: exposure to gaseous hydrogen at a pressure of 138 MPa and a temperature of 573 K for about 10 days. These conditions are used extensively in the literature and produce a hydrogen content of about 140 parts per million by weight [7]. The hydrogen content was verified by inert gas fusion on a number of hydrogen-precharged specimens, representing both type 316L and type 304L materials. Additional details of thermal precharging methods can be found in Refs. [7, 14].

3.0 RESULTS

3.1 Strength

The relationship between reduction of area (RA) and yield strength (YS) is plotted in Figure 1 for all the tested materials and conditions (note: hydrogen-precharged materials are plotted versus the yield strength of the same material/condition without hydrogen to aid comparison; high concentration of internal hydrogen increases YS by 10 to 15% [7, 14]). For non-charged materials with YS < 400 MPa, the RA values are typically 70 to 80%. With internal hydrogen, the RA values for these low-strength materials are generally greater than about 60%; however, RA values were as low as 40% in a few cases: one weld process and one material tested at low temperature. For non-charged type 304/304L materials with YS > 550 MPa, the measured RA is approximately 70%, which is the lower bound

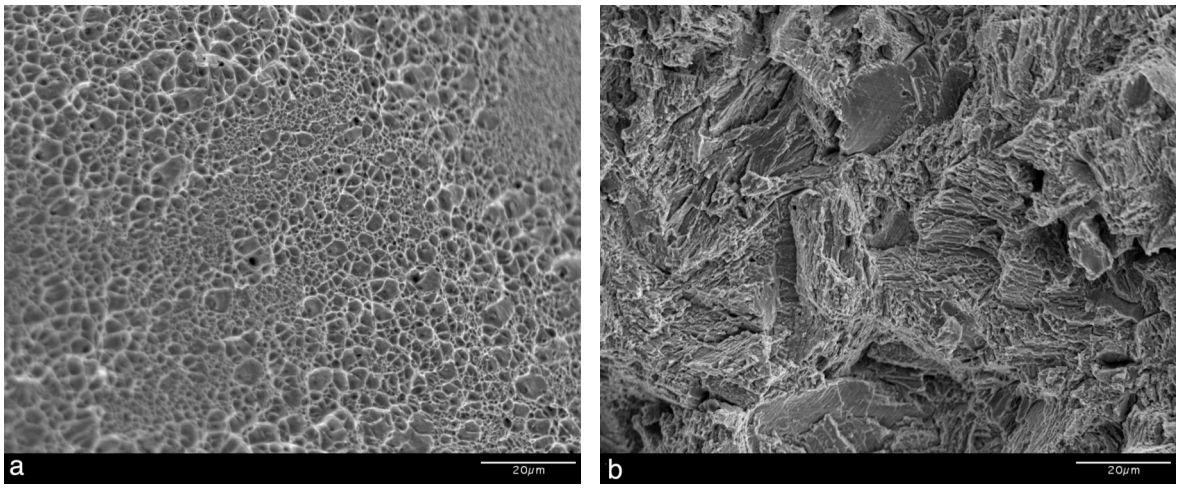

Figure 2. Fracture surfaces of type 304L tubing, material 6 tested at room temperature: (a) non-charged and (b) hydrogen-precharged.

observed for the low-strength conditions. With internal hydrogen, the RA for the high-strength materials is roughly 55% with the exception of the highest strength tubing (material 6), which shows RA of about 25%. Clearly, the high-strength materials result in greater loss of tensile ductility (RA) than the low-strength materials, but in all cases (except material 6) the RA is greater than 40% when hydrogen-precharged.

Differences in tensile ductility are also reflected in differences in the fracture features. Material 6, with the highest YS (763 MPa) and the lowest RRA (0.40), exhibits microvoid coalescence (MVC) for the non-charged condition similar to all the tested materials in the non-charged condition, but a corrugated morphology as well as planar facets for the hydrogen-precharged condition (Figure 2). These features on the fracture surface of the hydrogen-precharged material represent about 50% of the fracture surface; the remaining 50% is microvoid coalescence. In contrast, strain-hardened type 304L (material 2/condition A) shows less change on the fracture surface when hydrogen-precharged: while still dominated by MVC, the overall topography shows more nonuniform void structure. Annealed type 304L (material 2/condition F), on the other hand, features predominantly MVC for both non-charged and hydrogen-precharged conditions; this material/condition has the lowest yield strength (179 MPa) and relatively high RRA (0.82). Internal hydrogen reduces the dimple size, but does not otherwise alter the topography.

3.2 Nickel content

While there is a clear trend with strength, alloy content also plays an important role in hydrogen-assisted fracture. The effect of nickel content on tensile ductility is shown in Figure 4. In general for tubing materials tested at room temperature, the RA of hydrogen-precharged specimens is greater for materials with higher nickel content. The RRA for the highest nickel content (type 316L) is about 0.91 compared to an RRA of 0.40 for material 6 (type 304L) with the lowest nickel content; material 6 is also the tubing material with the highest yield strength. Materials with nickel content around 10 wt% (Figure 4) show RRA of around 0.75, suggesting a steeper dependence on nickel when the nominal nickel content is less than about 10 wt%. Figure 4 also shows RA to be effectively independent of nickel content for non-charged alloys.

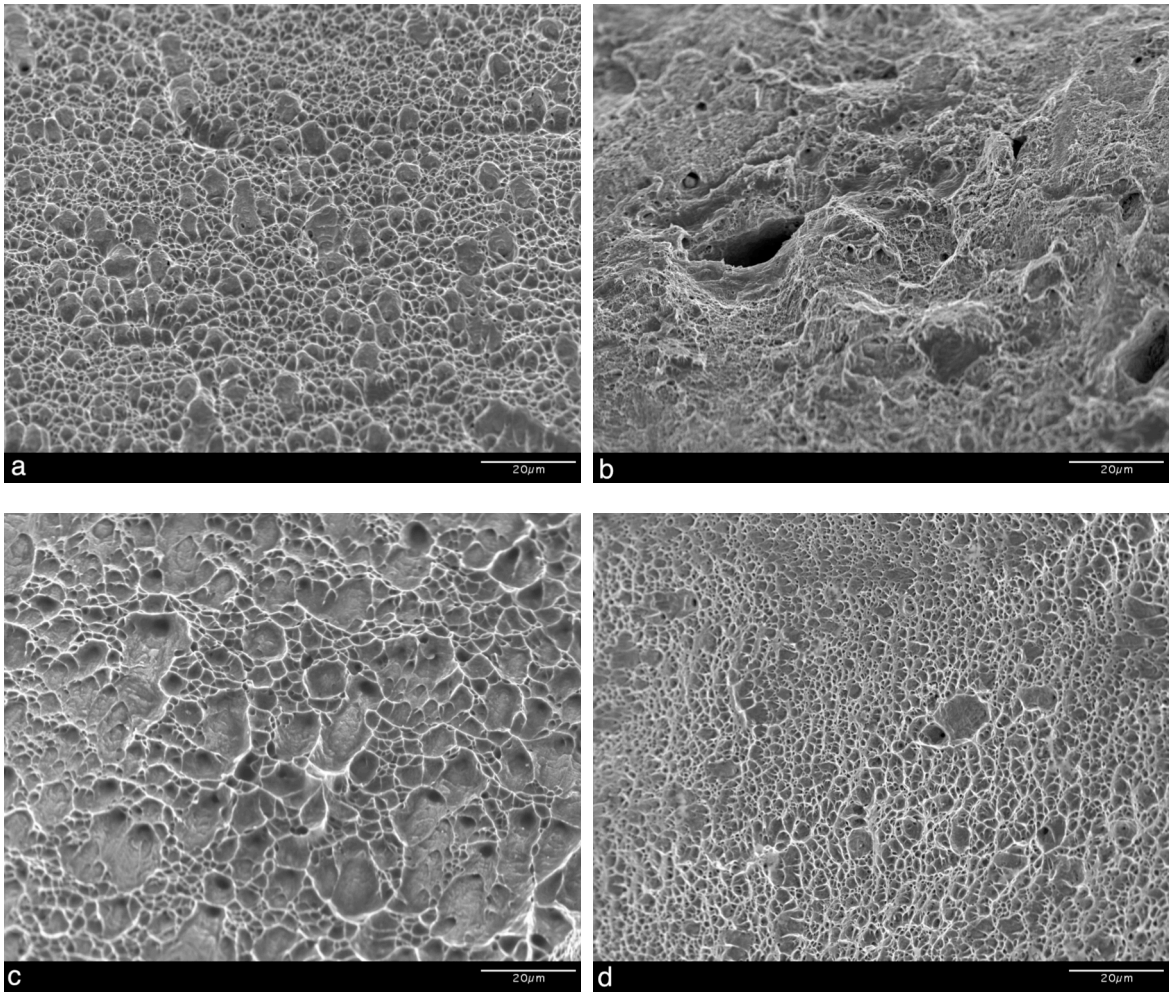

Figure 3. Fracture surfaces of type 304L tubing, material 2/condition A tested at room temperature: (a) non-charged and (b) hydrogen-precharged; material 2/condition F tested at room temperature: (c) non-charged and (d) hydrogen-precharged.

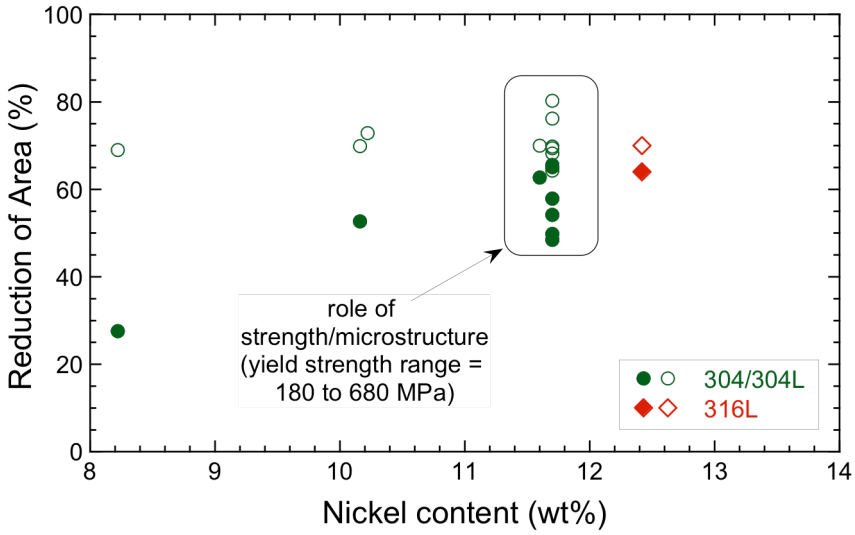

Figure 4. Reduction of area as a function of nickel content for all tested materials, with the exception of sensitized materials. Open symbols represent noncharged materials, while closed symbols represent hydrogen-precharged materials.

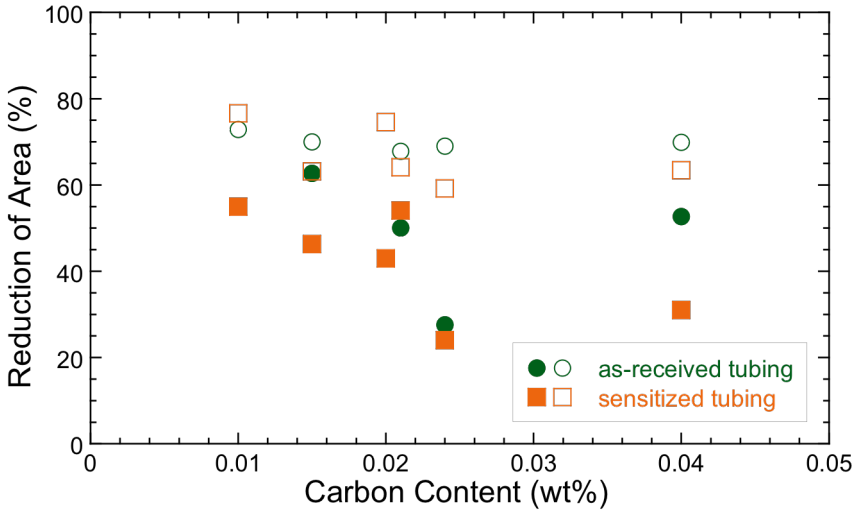

Figure 5. Reduction of area as a function of carbon content for type 304/304L as-received tubing and sensitized tubing. Open symbols represent non-charged materials, while closed symbols represent hydrogen-precharged materials.

3.3 Carbon content and sensitization

Prior to sensitization, carbon content does not appear to have a significant effect on the RA with or without hydrogen, see Figure 5. The RA of the non-charged tubing is essentially the same for all 6 tested compositions (one of the type 304L tubing materials was only tested after sensitization). The effect of internal hydrogen varies according to the strength and nickel trends as previously described and no correlation between hydrogen-assisted fracture and carbon content can be ascribed to the data without sensitization.

As mentioned above, the type 304/304L materials were subjected to a thermal treatment at a temperature of 998 K, which is within the sensitization range for these alloys. This sensitization treatment generally caused a slight reduction of RA for the non-charged material, as shown in Figure 5. The loss of ductility due to internal hydrogen after sensitization, however, is variable. For several of the materials, internal hydrogen does not seem to amplify the effects of sensitization, while for two materials in particular sensitization appears to exacerbate the effects of hydrogen. One of these materials is distinguished by its relatively high carbon content (material 4 is the only type 304 material in this report with >0.030 wt% carbon), while the other material is distinguished by its relatively high sulfur content (material 3 had 0.026 wt% sulfur compared to <0.007 wt% for all other alloys).

In general, sensitization does not change the fracture morphology of the L-grades; MVC remains the dominant fracture feature, Figure 6a. The combination of sensitization and hydrogen-precharging in these materials results in similar fracture morphology as hydrogen-precharging without prior sensitization: smaller dimples and occasional secondary cracking (Figure 6b). Sensitization of the type 304 tubing (material 4) produced a significant refinement of the dimple size and some secondary cracking as shown in Figure 7a. With the combination of sensitization and hydrogen-precharging, fracture of material 4 becomes intergranular (Figure 7b) with clear evidence of slip planes on the fracture facets. The high-sulfur alloy (material 3) also shows intergranular fracture over a portion of the fracture surface when hydrogen-precharged after sensitization, while classic MVC is observed on the fracture surface of the hydrogen-precharged material without sensitization (Figure 8). The intergranular facets of the sensitized and hydrogen-precharged high-sulfur alloy (material 3), however, are different from the high-carbon alloy (material 4): the fractured boundaries of the former are decorated with much larger indications of plasticity including dimples (Figure 8b).

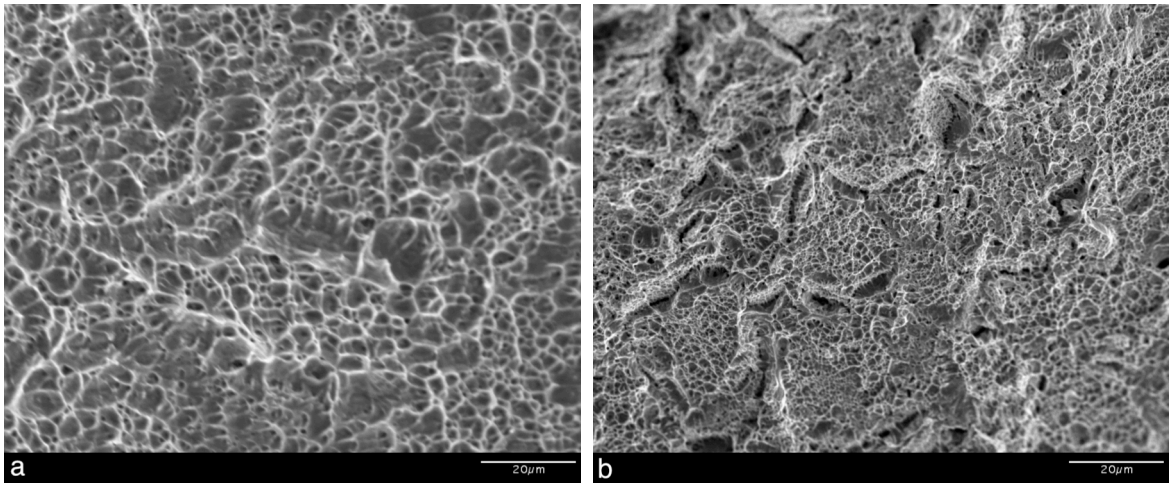

Figure 6. Fracture surfaces of type 304L tubing, material 2/condition A sensitized and tested at room temperature: (a) non-charged, and (b) hydrogen precharged.

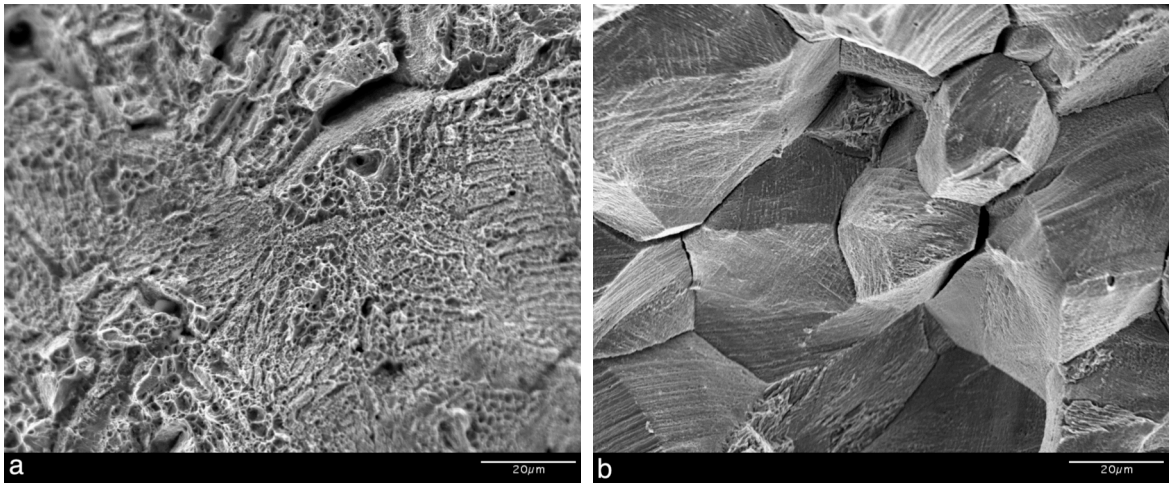

Figure 7. Fracture surfaces of type 304 tubing, material 4 sensitized and tested at room temperature: (a) non-charged, and (b) hydrogen-precharged).

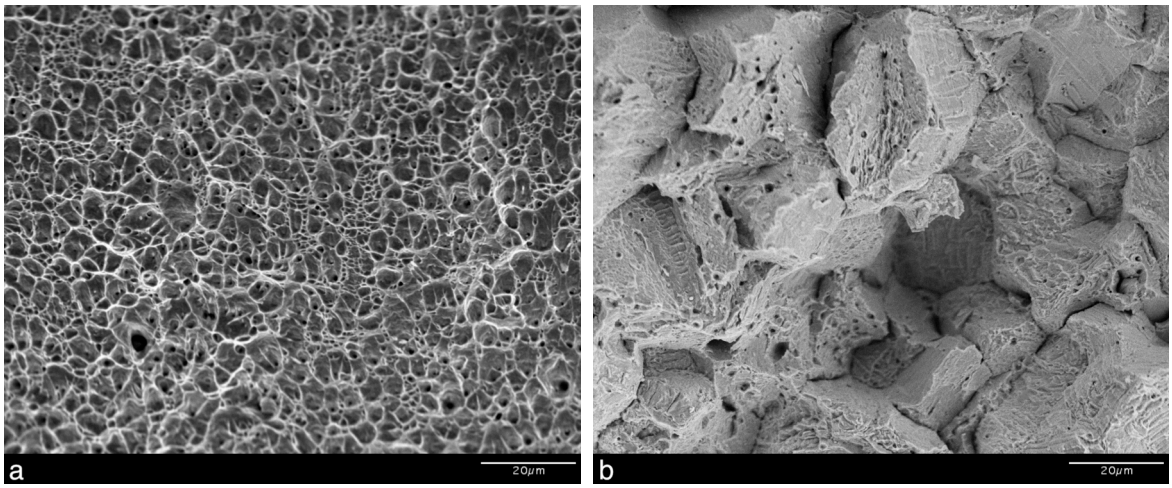

Figure 8. Fracture surfaces of type 304L tubing, material 3 tested at room temperature: (a) hydrogen precharged and (b) sensitized then hydrogen precharged.

3.4 Welding

The measured yield strength of the welded specimens is generally less than the tubing (the exception is welds in fully annealed tubing). This reduction of strength is quite significant for strain-hardened tubing (e.g., material 2/condition A). The RA values of the welded specimens are slightly greater than the tubing specimens, more so if the tubing is not in the annealed condition. Additionally, deformation appears to be relatively localized in the weld due to the lower strength of the weld fusion zone, thus accounting for the significantly lower elongation observed for the welded specimens [15], which is usually almost half of the elongation of the non-welded specimens. Welded specimens typically break in the fusion zone with the exception of welds in fully annealed tubing, specifically material 2/condition F. With internal hydrogen, tensile ductility is reduced in the welded specimens similar to the tubing with one exception: type 316L welded by process B. Weld process B shows marked reduction of tensile ductility when hydrogen precharged: the RRA is 0.59 for specimens welded by process B compared to 0.84 and 0.91 for specimens welded by process A and for type 316L tubing respectively.

The fracture surfaces from welded type 316L (process A) feature MVC with a uniform dimple size and equiaxed shape (Figure 9), although the dimples are much larger relative to the (non-welded) tubing. The welded type 304L specimens exhibit similar morphology to welded type 316L process A. Hydrogen precharging results in finer average dimple size and greater distribution of dimple sizes for all the welded specimens (Figures 9), similar to basic trends observed for the tubing. Fracture surfaces from type 316L specimens welded by process B show classic MVC in the absence of hydrogen. When hydrogen-precharged, however, these specimens (welded process B) show the largest changes in the fracture morphology among the welds, which is consistent with the lower measured RA.

3.5 Environmental temperature

Subambient testing increases the yield strength of non-charged type 316L tubing without affecting the tensile ductility. The RA of hydrogen-precharged specimens, however, is significantly reduced at low temperature relative to tests at room temperature. The tensile ductility for both the welded type 316L tubing (process A) and the non-welded tubing, on the other hand, are essentially the same: 50% and 48% for the welded and non-welded specimens respectively (hydrogen precharged and tested 223 K). The RRA at 223 K is 0.77 and 0.69 for the welded and non-welded specimens respectively.

The fracture surfaces of the welded type 316L specimens tested at low temperature (Figures 9c and 9d) show features similar with the non-welded tubing. The noncharged welded specimens exhibit MVC, while the hydrogen-precharged welded specimens exhibit a few flat, facetted regions and reduced dimple size when tested at a temperature of 223 K (Figure 9d).

4.0 DISCUSSION

4.1 Strength

The relationship between higher strength and increased hydrogen embrittlement has been discussed by Louthan [10] and is attributed to higher strength materials having more dislocations and higher internal stresses. The RRA of material 2 in condition A and B is close to 0.7, while for the other conditions RRA > 0.8, suggesting strain-hardened microstructures are more susceptible to hydrogen-assisted fracture than recovered microstructures. Additionally, recrystallization (conditions D and E) and grain growth (condition F) processes did not significantly affect susceptibility (or resistance) to hydrogen-assisted fracture. Previous work on annealed and strain-hardened type 316/316L austenitic stainless steels [7], however, suggests yield strength did not impact susceptibility to hydrogen. While the results here provide a little more insight on the role of strength, the results for tubing are consistent with previous assessment: strength is not a strong determining factor in ductility loss of hydrogen-charged materials tested in uniaxial tension.

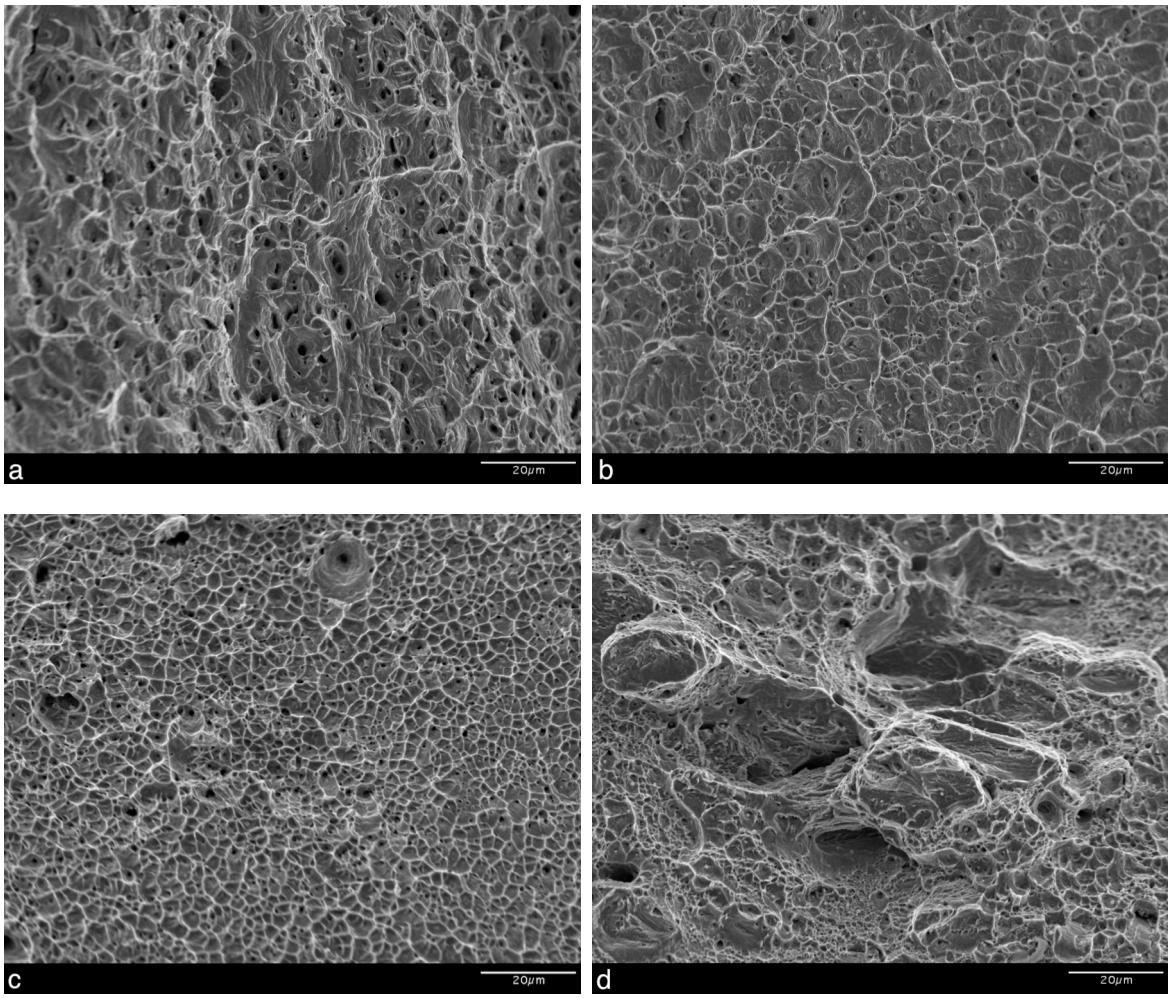

Figure 9. Fracture surfaces of welded type 316L austenitic stainless steel tubing (weld process A), tested at room temperature: (a) non-charged and (b) hydrogen-precharged; and tested at temperature of 223 K: (c) non-charged and (d) hydrogen-precharged.

The fractography also supports the limited role of strength on hydrogen-assisted fracture. Comparison of the fracture surfaces in Figure 3 for strain-hardened (material 2/condition A) and annealed (material 2/condition F) type 304L shows a similar characteristic of MVC. This similarity can be contrasted with the fracture surface of material 6, which shows a significant change in fracture surface character in the presence of hydrogen (Figure 2). While material 6 is the highest strength tubing tested in this report, the change in fracture surface and the much lower RRA (=0.4) do not follow the strength trend established by the other materials as shown in Figure 1. The observed lower fracture resistance of material 6 compared to material 2 is explained by composition in the next section.

4.2 Composition and environmental temperature

The correlation of hydrogen effects with nickel content (Figure 4) has been established by a large number of studies [5, 7, 8]. The relatively wide variation of results with a nickel content of 11.7 wt% is explained by changes in strength as discussed in the previous section. The fractography results are also consistent with previous study. Difference between the fracture morphology in Figures 2 and 3 are attributed to nickel content (both materials are strain-hardened). Although the void structure is non-uniform, Figure 3b shows MVC for hydrogen-precharged type 304L with high nickel content (11.7 wt%, material 2), while Figure 2b shows a corrugated surface with some faceting for hydrogen-precharged type 304L with comparatively low nickel content (8.2 wt%, material 6). The latter features are hypothesized to be the result of enhanced localized plasticity promoting void formation at the intersection of slip bands or slip planes as well as twin boundary fracture. In short, materials are more

sensitive to hydrogen when their deformation can be characterized by localized deformation (such planar slip). Low nickel content in austenitic stainless steels typically results in lower stacking fault energy, which inhibits cross slip and promotes planar deformation structures, leading to enhanced sensitivity to hydrogen [7, 8, 16]. It is important to note other characteristics of the material and environmental conditions can enhance localized deformation and appear to correlate with greater hydrogen sensitivity, such as coherent precipitation and short-range ordering. Subambient temperature is known to enhance hydrogen-assisted fracture of austenitic stainless steels [3, 8, 17]; this observation has been attributed to the combined effects of hydrogen and temperature on localization of plasticity in these materials.

Carbon content does not correlate with the observed effects of hydrogen. It has been suggested in the literature that decreased austenite stability can be related to increased hydrogen sensitivity, which would imply a strong role of carbon on hydrogen effects. Such effects of carbon in solution, however, have not been exposed in the literature. Carbon precipitation due to poor material processing or by sensitization, on the other hand, appears to promote hydrogen effects. These phenomena can be explained by the effects of microstructure on the character of deformation, thus influencing hydrogen-assisted fracture.

4.3 Sensitization

Sensitization in austenitic stainless steels generally refers to thermal exposure that causes carbide precipitation along grain boundaries, leading to greater susceptibility to intergranular attack in corrosive environments. Sensitization has been demonstrated to exacerbate hydrogen-assisted fracture in austenitic stainless steels [6, 11-13]. In the tested type 304L tubing, the RRA is similar with and without sensitization. Indeed, the L-grades are intended for service when the materials may be sensitized, such as during welding or high-temperature service. Thus, relatively small effects of sensitization on the microstructure of the L-grades might be expected, resulting in limited impact on hydrogen resistance as measured by tensile ductility (RA). Two materials, on the other hand, showed a strong enhancement of the hydrogen effects after sensitization: material 4 (0.04 wt% carbon) and material 3 (0.015 wt% carbon). The RRA of non-sensitized material 4 is 0.75, however, when sensitized, the RRA is reduced to 0.49. Material 4 likely forms carbides at the grain boundaries when sensitized leading to intergranular fracture as shown in Figure 6. Grain boundary carbides are implicated in lower austenite stability due to the loss of chromium as well as enhanced localized plasticity due to either or both carbide precipitation and lower alloy content [6, 12]. Material 3 is distinguished from the other L-grades by high sulfur content. Sulfur is known to embrittle grain boundaries of ferritic steels and nickel. We speculate high sulfur can “sensitize” grain boundaries of austenitic stainless steels to hydrogen-assisted fracture, leading to lower ductility and intergranular fracture, as shown in Figure 8.

4.4 Welding

The welded specimens generally showed similar or greater ductility than the base materials from which they were produced. For the high-strength tubing in particular, this greater ductility is likely a reflection of the significantly reduced YS of the welded specimens relative to the tubing. After hydrogen precharging, the welded specimens generally demonstrated RA consistent with their strength (Figure 1); in other words, the RRA of the welded specimens is greater than high-strength base materials. The welds of low-strength type 316L (process A) are slightly more susceptible to hydrogen in terms of RRA, although the RA of the hydrogen-precharged welded specimen is the same as the base material. The lower RRA of welded type 316L may indicate greater susceptibility of the weld microstructure to hydrogen, although a modest one. The importance of the weld microstructure becomes evident when comparing the large reduction of RA for the hydrogen-precharged, welded specimens of type 316L produced by process B. Clearly, welding can produce a range of microstructures with significant variation in hydrogen susceptibility. More work is underway to better understand these microstructural differences. However, it is important to note, despite a large change

of ductility due to hydrogen, welded type 316L specimens produced by process B remained very ductile when hydrogen-precharged: RA> 40%.

Type 304L specimens welded from annealed tubing (material 2/condition F) differ from the other welded tubing because these specimens often broke outside the weld fusion zone (both non-charged and hydrogen-precharged). This observation is consistent with the work of Naumann and Michler [2]. In the case of "dead-soft" tubing (such as condition F), the strength of the weld material may be greater than the base material, or the slightly greater thickness of the weld may reduce the stress in this region, thus the necking instability is transferred to the base material. Fracture in the base material of the low-strength tubing clearly differs from higher-strength tubing, where necking and fracture were always observed in the weld material. In any case, the RA of specimens welded from annealed type 304L (material 2/condition F) is essentially the same as the RA of the base material.

5.0 CONCLUSIONS

The strength and composition of austenitic stainless steels influence hydrogen-assisted fracture of these alloys. Environmental effects, such as sub-ambient temperature, reduce the resistance of these alloys to the effects of hydrogen. Segregation and second phases, such as those formed during sensitization, can also negatively impact resistance to hydrogen-assisted fracture in tensile testing. From tensile testing results on hydrogen-precharged tubing and orbital tube welds, the following conclusions were drawn:

- Strain-hardened microstructures (YS > 600 MPa) decrease resistance to hydrogen-assisted fracture in tensile tests. Recovered and recrystallized microstructures, however, show greater resistance to hydrogen effects and similar values of RRA for a range of YS.

- Nickel content is the dominant material variable for resistance to ductility loss in tension. The role of carbon content could not be correlated to the effects of hydrogen in this work. When sensitized, the low-carbon grades showed similar tensile ductility loss as the non-sensitized materials. The type 304 material (highest carbon content), however, showed enhanced tensile ductility loss due to the combined effects of sensitization and hydrogen.

- Orbital tube welds can be as resistant to hydrogen as the tubing base material. However, the compatibility of the welds is dependent on the welding parameters; here type 316L welds produced by the same process but with different parameters showed significantly different loss of ductility. Despite greater ductility loss in some cases, all of the tested welds showed relatively high ductility when hydrogen precharged (RA > 40%).

In summary, high-quality type 304L and type 316L austenitic stainless steel tubing show acceptable ductility (RA > 40%) for pressure applications when precharged with high hydrogen concentrations and tested at room temperature. Welded tubing also performs well under these conditions.

ACKNOWLEDGEMENTS

Sandia National Laboratories is a multi-program laboratory managed and operated by Sandia Corporation, a wholly owned subsidiary of Lockheed Martin Corporation, for the U.S. Department of Energy's National Nuclear Security Administration under contract DE-AC04-94AL85000.

REFERENCES

1. Jackson, H.F., Nibur, K.A., San Marchi, C., Puskar, J.D. and Somerday, B.P. Hydrogen-assisted crack propagation in 304L/308L and 21Cr-6Ni-9Mn/304L austenitic stainless steel fusion welds. *Corros Sci,* **60**, 2012, 136-144.
2. Naumann, J. and Michler, T. Hydrogen enviroment embrittlement of orbital welded austentic stainless steels at -50˚C. *Int J Hydrogen Energy,* **34**, 2009, 6478-6483.

3. Sun, D., Han, G., Vaodee, S., Fukuyama, S. and Yokogawa, K. Tensile behaviour of type 304 austenitic stainless steels in hydrogen atmosphere at low temperatures. *Mater Sci Technol,* **17**, 2001, 302-308.
4. Caskey, G.R. Hydrogen Compatibility Handbook for Stainless Steels (DP-1643). EI du Pont Nemours, Savannah River Laboratory, Aiken SC (June 1983).
5. Zhang, L., Wen, M., Imade, M., Fukuyama, S. and Yokogawa, K. Effect of nickel equivalent on hydrogen gas embrittlement of austenitic stainless steels based on type 316 at low temperatures. *Acta Mater,* **56**, 2008, 3414-3421.
6. Han, G., He, J., Fukuyama, S. and Yokogawa, K. Effect of strain-induced martensite on hydrogen environment embrittlement of sensitized austenitic stainless steels at low temperatures. *Acta Mater,* **46**, 1998, 4559-4570.
7. San Marchi, C., Somerday, B.P., Tang, X. and Schiroky, G.H. Effects of alloy composition and strain hardening on tensile fracture of hydrogen-precharged type 316 stainless steels. *Int J Hydrogen Energy,* **33**, 2007, 889-904.
8. San Marchi, C., Michler, T., Nibur, K.A. and Somerday, B.P. On the physical differences between tensile testing of type 304 and 316 austenitic stainless steels with internal hydrogen and in external hydrogen. *Int J Hydrogen Energy,* **35**, 2010, 9736-9745.
9. San Marchi, C., Yang, N.Y.C., Headley, T.J. and Michael, J. Hydrogen-assisted fracture of low nickel content 304 and 316L austenitic stainless steels. in: 18th European Conference on Fracture (ECF18), Dresden, Germany, 30 August - 3 September 2010.
10. Louthan, M.R., Caskey, G.R., Donovan, J.A. and Rawl, D.E. Hydrogen Embrittlement of Metals. *Mater Sci Eng,* **10**, 1972, 357-368.
11. Thompson, A.W. The Behavior of Sensitized 309S Stainless Steel in Hydrogen. *Mater Sci Eng,* **14**, 1974, 253-264.
12. Briant, C.L. Hydrogen Assisted Cracking of Sensitized 304 Stainless Steel. *Metall Trans,* **9A**, 1978, 731-733.
13. Minkovitz, E. and Eliezer, D. Grain-size and heat-treatment effects in hydrogen-assisted cracking of austenitic stainless steels. *J Mater Sci,* **17**, 1982, 3165-3172.
14. San Marchi, C., Balch, D.K., Nibur, K. and Somerday, B.P. Effect of high-pressure hydrogen gas on fracture of austenitic steels. *J Pressure Vessel Technol,* **130**, 2008, 041401.
15. San Marchi, C., Hughes, L.A., Somerday, B.P. and Tang, X. Hydrogen-assisted fracture of type 316L tubing and orbital welds (PVP2013-97538). in: Proceedings of PVP-2013: ASME Pressure Vessels and Piping Division Conference, Paris, France, 14-18 July 2013.
16. San Marchi, C., Nibur, K.A., Balch, D.K., Somerday, B.P., Tang, X., Schiroky, G.H. and Michler, T. Hydrogen-assisted fracture of austenitic stainless steels. in: BP Somerday, P Sofronis and R Jones, editors. Effects of Hydrogen on Materials. Proceedings of the 2008 International Hydrogen Conference (Moran WY, 2008). Materials Park OH: ASM International (2009) p. 88-96.
17. San Marchi, C., Somerday, B.P., Tang, X. and Schiroky, G.H. Hydrogen-assisted fracture of type 316 stainless steel at subambient temperature (PVP2008-61240). in: Proceedings of PVP-2008: ASME Pressure Vessels and Piping Division Conference, Chicago IL, 27-31 July 2008.